GRAVITY SIGNATURE OF VALLES SCHRÖTERI AND THE POSSIBILITY OF DETECTING LAVA TUBES ASSOCIATED WITH SINUOUS RILLES. K. Gansler[1], L. Montési[1] and V. Lekić[1], [1]University of Maryland, College Park, Department of Geology

Introduction: The gravity field of the Moon is now known with very high resolution and precision as a result of NASA's Gravity Recovery And Interior Laboratory (GRAIL) mission. [1] presents a gravity field solution with a maximum order l of 1200 consistent with a wavelength of 0.15° or approximately 9 km at the Moon's equator. This high resolution opens the possibility of identifying the gravity signature of small geological features. We focus here on the possible gravity signature of sinuous rilles. Their likely origin as eroded lava channels or collapsed lava tubes suggests that they may be spatially associated with lava tubes or other underground voids of high interest for future lunar exploration. This study examines whether gravity data can provide new constraints on the structure of sinuous rilles to complement previous analyses that used visible and topographic data [e.g., 2].

The difference between a free-air gravity field and the predicted field based on topography, known as the Bouguer anomaly, has the potential to reveal subsurface features such as lava tubes. Based on this principle, Bouguer gravity anomalies are often interpreted in terms of regional differences in crustal density or thickness. Here, we compare the free-air gravity signals observed above specific geological features, sinuous rilles with those expected from their topographic profiles.

Sinuous rilles may have formed by the downward erosion by a lava flow or by the collapse of a lava tube. In the latter case, sinuous rilles are expected to be spatially associated with remaining lava tubes or tube segments [3]. Steep-sided pits on the floor of some rilles provide evidence for the presence of such underground voids [4, 5]. [6] proposed that linear gravity anomalies indicate the presence of large voids beneath some sinuous rilles, but these voids would be wider than 10 km, much larger than the lunar pits, terrestrial lava tubes, or the rilles themselves. That study was based on gradiometry and cross-correlation techniques and relied on the Bouguer gravity anomalies determined from spherical harmonics analysis to determine if subsurface voids exist in the study area. To complement that work, we study here the free-air gravity field in the vicinity of the widest lunar sinuous rille, Valles Schröteri, and compare it with the expected signal based on the rille topography, in order to determine if the rille is collocated with an additional mass deficit that could indicate the presence of a lava tube.

Analysis: Because the width of even the largest sinuous rille is smaller than the resolution of global gravity anomaly maps, we focused our investigation on the widest rille, Valles Schröteri, just northwest of Aristarchus and Herodotus Craters in the region between Oceanus Procellarum and Mare Imbrium. Fig. 1 shows that the rille is associated with a negative free-air gravity anomaly in GRAIL's *GRGM1200A* free-air gravity anomaly map [1]. We determine here if that anomaly can be explained by the Valles Schröteri or if it requires the presence of additional void spaces.

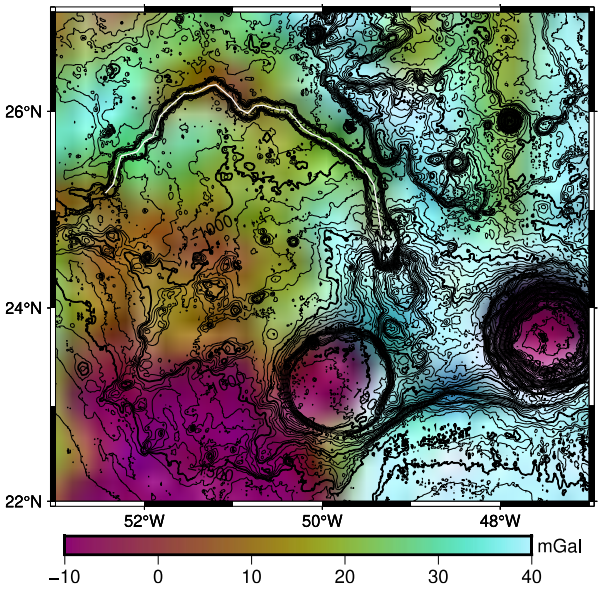

Figure 1: Free air anomaly at Valles Schröteri over topographic contours. The path of the rille is shown with a white line. A region of strong negative gravity is visible at the curve in the northernmost area of the rille. Data from [1] and [7].

We traced the axis of the Valles Schröteri (Fig. 1) using Lunar Reconnaissance Orbiter Camera mosaics. From the merged LRO LOLA – SELENE Kaguya TC *SLDEM2015* 512-pixel-per-degree lunar digital elevation model [7] and *GRG1200A*, we extracted 300-km-long tracks centered on points separated by 0.01° along the track of the rille. The free air gravity anomaly along each track is denoted as $g_{\mathrm{FA}}(x)$, where x is the distance from the center of the valley. For each track, the edges of the valley were detected using the curvature of the topographic profile and the cross-sectional area A was calculated by integrating the topography between these edges (Fig. 2). Tracks where this algorithm failed to correctly identify the edges of Valles Schröteri were removed from the analysis, leaving a total of 247 tracks.

The observed gravity anomaly is compared with the gravity field produced by a straight filament with linear mass density λ meant to represent an idealized version of the valley. The gravity signal associated with such a

filament is $g_{\mathrm{th}} = \lambda g_{\mathrm{f}}$, with g_{f} the gravity anomaly arising from a filament with unit λ

$$g_{\mathrm{f}} \equiv \frac{2G}{\sqrt{h^2 + x^2}}$$

Here, h is the distance between the top of the rille and the radius at which GRGM1200A is defined (1,738 km), and G is the gravitational constant.

Both this theoretical gravity signal and the observed gravity signal are then bandpass filtered using a zero-phase first order Butterworth filter. The high-pass corner spatial frequency corresponds to a wavelength of 9 km, and therefore the shortest wavelengths present in the l = 1200 observed free-air gravity field [1]. A low-pass corner corresponding to a wavelength of 54.6 km removes large-scale signals from both the observed gravity field and the theoretical gravity values to isolate the signal from the rille.

If the filament model is an adequate representation of the observed gravity anomaly, g_{FA}, a scaled g_{f} would be expected to fit the observations to within a constant offset, g_0 that accounts for any large-scale observed signals other than the rille itself:

$$g_{\mathrm{FA}} = g_0 + \lambda g_{\mathrm{f}}$$

We determine the best-fitting values of g_0 and λ using MATLAB's *fit* function and report the density of the material missing in the rille

$$\rho = -\lambda / A$$

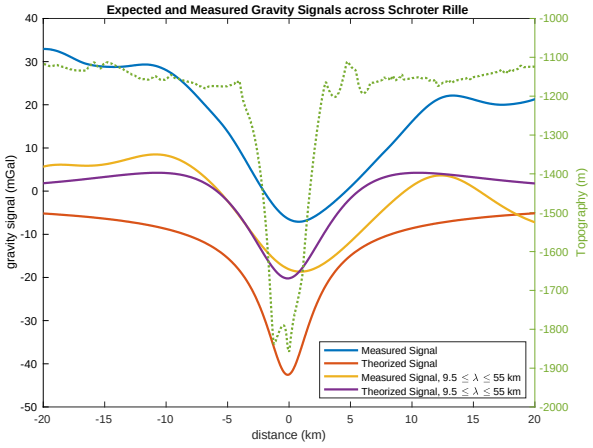

Figure 2: Example gravity and topography profiles used for analysis along with the theorized signal arising from a straight filament. The cross-sectional area of the rille is highlighted in grey with the topography along the cross-section.

Discussion: In the case of the track shown in Fig. 2, the observed free-air anomaly (blue and yellow) has a pronounced minimum above Valles Schröteri (topography in green). After bandpass filtering (purple), its width is similar to that of the filament model (red). The best-fit λ implies a density deficit of 2200 kg/m^3, and a small value of g_0 (1 mGal) suggests that the filament model adequately represents the observed gravity anomaly.

The bulk lunar crustal density has been estimated to be 2550 kg m^{-3} [1] but can be as low as 2,200 in highland regions and more than 3,300 kg m^{-3} in the densest basalts [8]. The track in Fig. 2 can therefore be fully explained by the mass deficit associated with the topographic expression of Valles Schröteri. Therefore, no lava tube can be resolved in this location. Tracks with similar characteristics are highlighted in green in Fig. 3.

However, other tracks require density deficits as high as 5,000 kg m^{-3}. These profiles (red in Fig. 3) are located where the free-air gravity anomaly is particularly large in Fig. 1. Signal amplitude may imply that there is an underground lava tube as large as Valles Schröteri in this region or that the crust directly beneath the valley has anomalously high porosity.

Additional profiles do not show the kind of gravity anomaly minimum expected from the filament model and are not analyzed further (yellow in Fig. 3).

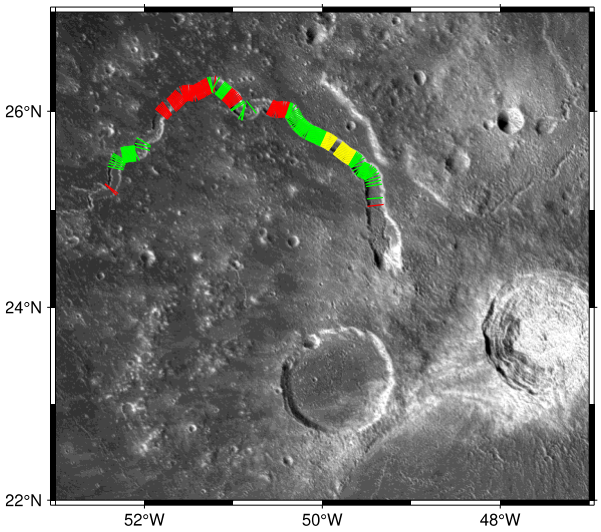

Figure 3: Visible image of Valles Schröteri with the location of analyzed tracks. Only the central portion of each track is shown here for clarity. Tracks that can be explained with the signal for Valles Schröteri alone are shown in green, while those in red require additional voids near the rille. The tracks in yellow cannot be explained by our filament model.

References: [1] Goossens S. et al. (2021) *ESS*, DOI: 10.1029/2021EA001695. [2] Hurwitz D. M. et al. (2013) *PSS*, DOI: 10.1016/j.pss.2012.10.019. [3] Greeley R. (1971) *Science*, DOI: 10.1126/science.172.3984.722. [4] Robinson et al. (2019) *PSS*, *69*, 18-27, DOI 10.1016/j.pss.2012.05.008. [5] Sauro, et al. (2020) *ESR*, DOI 10.1016/j.earscirev.2020.103288. [6] Chappaz L. et al. (2016*) GRL*, DOI: 0.1002/2016GL071588 [7] Barker, M. K. et al. (2016) *Icarus*, DOI: 10.1016/j.icarus.2015.07.039 [8] Kiefer W. S. et al. (2012) *GRL*, DOI: 10.1029/2012GL051319